Supporting information

Asymmetric non-fullerene acceptors with imide-containing end group for organic solar cells

Shiling Shi,[1] Shimin Zhang,[2] Xiang Yao,[1,3*] Kaihu Xian,[4] Dexia Han,[4] Yuxuan Zhu,[5] Yanru Li,[1] Xueyang Tu,[1] Zheng Tang,[5] Long Ye,[4] Hongliang Zhong,[2*] and Zhuping Fei[1, 3*]

[1)] Institute of Molecular Plus and Tianjin Key Laboratory of Molecular Optoelectronic Science, Tianjin University, Tianjin 300072, P. R. China

[2)]School of Chemistry and Chemical Engineering, Shanghai Key Lab of Electrical Insulation and Thermal Aging, Shanghai Jiao Tong University, Shanghai 200240, P. R. China

[3)]Haihe Laboratory of Sustainable Chemical Transformations, Tianjin 300192, P.R. China

[4)]School of Materials Science and Engineering, Tianjin University, Tianjin 300350

[5)]Center for Advanced Low-dimension Materials, State Key Laboratory for Modification of Chemical Fibers and Polymer Materials, College of Materials Science and Engineering, Donghua University, Shanghai 201620, P. R. China

Table of Contents

1. Experimental Section

1.1 Methods and measurements

^{1}H and ^{13}C NMR spectra were recorded on a Bruker AV 600 MHz or JEOL/JNM-ECZ600R/S1 600 MHz spectrometer. Mass spectrometry (MS) (MALDI-TOF) results were performed with Bruker FLEX-PC rapifleX instrument.

UV-visible absorption spectra were obtained on a UV-vis-NIR spectrometer (UV-3700). Atomic force microscopy (AFM) measurements were performed under ambient conditions using a Digital Instrument Multimode Nanoscope IIIA operating in the tapping mode. Thickness of the blend films was determined by a Dektak XT surface profile meter. Thermogravimetric analysis (TGA) was performed on PerkinElmer Pyris 1 thermogravimetric analyzer under a nitrogen atmosphere at a heating rate of 10 °C/min to record TGA curves.

Electrochemical properties of the acceptors were evaluated by cyclic voltammetry (CV) using a CHI 630A Electrochemical Analyzer in degassed CH_3CN. The supporting electrolyte was tetrabutylammonium phosphorus hexafluoride (Bu_4NPF_6, 0.1 M). A glass carbon disk, a Pt wire and a saturated Ag/AgCl electrode were selected as the working electrode, counter electrode and reference electrode, respectively. The samples under test were prepared by drop-casting the freshly prepared chloroform solution (~10 mg/mL) of the acceptors atop the well-polished working electrode. The HOMO and LUMO energy levels (E_{HOMO} and E_{LUMO}) of the acceptors were derived according to the following equation[1]:

$$E_{HOMO/LUMO} = -e(\varphi_{ox/red} + 4.8 - \varphi_{Fc/Fc+}).$$

Here, φ_{ox} and φ_{red} represented the onset of the first oxidation and reduction peaks, respectively, ferrocene-ferrocenium (Fc/Fc^{+}) redox couple was applied to calibrate the potential before the test and $\varphi_{Fc/Fc+}$ was estimated to be 0.43 V in our test.

1.2 Quantum Calculation

Density functional theory (DFT) calculations were performed using the Gaussian 16 program with B3LYP exchange-correlation functionality. All-electron triple-ξ valence basis sets with polarization functions (SVP) were used for all atoms. Geometrical optimizations were performed with full relaxation of all atoms. It should notice that the calculations were performed in gas phase without solvent effects. Vibrational frequency calculations were performed to check that the stable structures had no imaginary frequency. The alkyl substituents on the core were reduced to methyl groups for simplification as the alkyl substituents have negligible impact on the conformations and frontier energy levels of the molecules.

1.3 Fabrication and Characterization of the OSCs

OSCs were fabricated with the device configuration of ITO/PEDOT:PSS/active layer/PFNBr/Ag through the following steps. The indium tin oxide (ITO) glass was precleaned sequentially in an ultrasonic bath of isopropanol alcohol, acetone, detergent, and deionized water sequentially each for 20 min. The substrates were then treated with O_2 plasma for 10 min. A PEDOT:PSS (Heraeus Clevios PVP AI 4083, filtered at 0.45 μm) thin film was spin-coated on top of the precleaned ITO substrates at 4000 rpm for 30 s to obtain a film thickness of 40 nm and annealed at 150 °C for 15 min on a hot-plate before being transferred into a glovebox. A mixture of PM6 and BTP-IIC-2Cl/BTP-IIC-BO-2Cl in chlorobenzene (CB) (polymer concentration of 8.5 mg mL^{-1}) was stirred at 55 °C for 12 hours to ensure sufficient dissolution and then spin-coated on the top of the ITO/PEDOT:PSS layer. Afterward, PFNBr was spin-coated from its methanol solution (0.5 mg/mL) at 3000 rpm for 30 s, and ~ 60 nm Ag electrode were then evaporated onto the PFNBr layer then thermal evaporation at a vacuum pressure of 2×10^{-6} mbar. Photovoltaic device area was measured to be 0.035 cm^2. The *J-V* curves of solar cells were recorded in glove box at approximately 25 °C using an instrument from Enli Technology Ltd., Taiwan (SS-F5-3A) under AM 1.5G illumination from AAA class solar simulator, with a light intensity of 100 mW cm^{-2} calibrated with a standard reference Si photovoltaic cell). External quantum efficiency (EQE) measurements were conducted in air without encapsulation. The EQE data were obtained using a solar cell spectral response measurement system (QE-R3018, Enli Technology Co. Ltd), and the intensity was calibrated with a standard reference Si photovoltaic cell.

1.4 Fabrication and characterization of the hole/electron-only devices

Hole and electron-only devices with a structure of ITO/PEDOT:PSS/active layer/MoO_3/Ag and ITO/Al/active layer/Al were fabricated, respectively. A solution of PM6 and acceptors in chlorobenzene (CB) was spin-coated on the top of PEDOT:PSS or Al thin film to form the active layer, then MoO_3 (9 nm)/Ag was thermally evaporated at a pressure of 2×10^{-6} mbar through a shadow mask. Dark *J-V* curves of the hole/electron-only devices were measured and charge mobilities were calculated by the space-charge-limited-current (SCLC) method. Dark *J-V* curves were fitted by using the Mott-Gurney equation[2]: $J = 9\varepsilon_o\varepsilon_r\mu V/8d^3$, where J is the space charge limited current, ε_0 is the vacuum permittivity ($\varepsilon_o = 8.85 \times 10^{-12}$ F/m), ε_r is the permittivity of the active layer ($\varepsilon_r \approx 3$), μ is charge mobility, and d is the thickness of the active layer.

1.5 Energy loss determination

The highly sensitive EQE (sEQE) spectra are measured using a halogen lamp (LSH-75, Newport), a monochromator (CS260-RG-3-MC-A, Newport), a chopper with a frequency of 137 Hz and a set of long

pass filters (600, 900 and 1100 nm) to eliminate the overtones. The electrical signals from the devices were received by a front-end current amplifier (SR 570, Stanford) and a phase-locked amplifier (SR 830, Newport). Light intensity was calibrated by a silicon detector (Hamamatsu S1337-1010BR). Electroluminescence spectra (EL) were measured using a Kymera-328I spectrometer and an EMCCD (DU970P-1.7) camera from Andor Technology. The E_g of acceptors are determined by the intersection of absorption and photoluminescence curves of the PM6:BTP-IIC-2Cl and PM6:BTP-IIC-BO-2Cl blends.

The measured EQE spectra were combined with the EQE spectra calculated from the EL spectra, using the reciprocal relation between absorption and emission. The E_{CT} was determined using Gaussian fitting[3]:

$$EQE_{PV} = (f*E)/\mathrm{sqrt}(4\pi kT\lambda)\exp(-(E_{CT}+\lambda-E)_2/(4kT\lambda)) \quad (1)$$

where E is the energy of photons, k is the Boltzmann constant, E_{CT} is the energy of CT state, is the reorganized energy, and T is temperature. f is a prefactor related to the density and the absorption oscillator strength of CT states.

EL spectra was measured using a home-built set-up. A Keithley 2400 was used to inject current into the solar cells in dark, and a Keithley 6482 was used to record the photocurrent from a Si detector (HAMAMATSU S1337-1010BR). We have also evaluated ΔV_{nr}, using the EQE spectra of the solar cells measured by a sensitive EQE setup.[4-7] First, we calculated the radiative limit for the dark saturation current and the radiative recombination limit for V_{OC}, using the equations:

$$J_{0,rad} = q\int EQE(E)\cdot BB(E)dE \quad (2)$$

$$V_{oc,rad} = \frac{kT}{q}\ln\left(\frac{J_{SC}}{J_{0,rad}}\right) \quad (3)$$

where BB is the blackbody spectrum at 300 K. Then, we determined ΔV_{nr} using the equation:

$$\Delta V_{nr} = V_{oc,rad} - V_{oc} \quad (4)$$

2. **Synthetic Section**

Materials. Unless otherwise noted, all chemicals were obtained from J&K Scientific, Energy Chemical，Solarmer or Titan and used without further purification. All other reagents and solvents were purchased commercially as analytically pure and used without further purification. Compound **1a,** Compound **1b,** Compound **2** and PM6 were synthesized according to previously reported methods.[8-10]

Synthetic details and characterizations

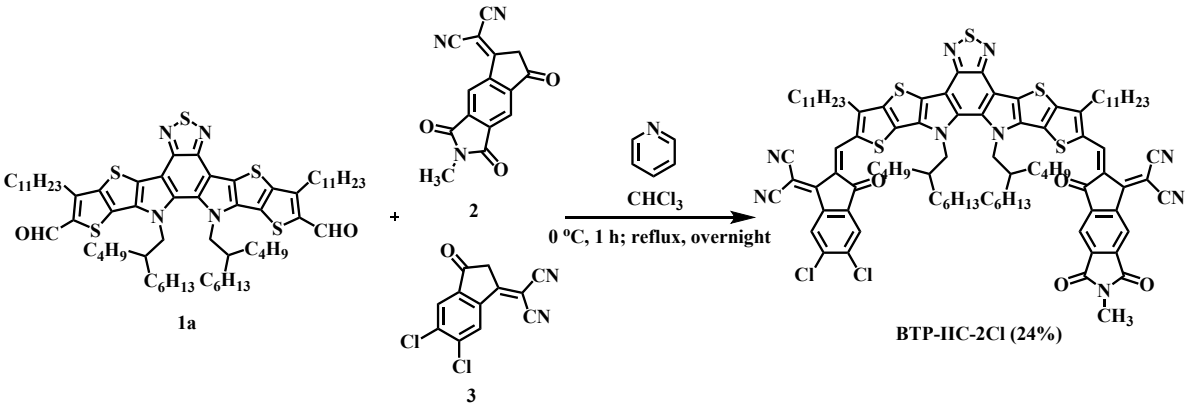

Synthesis of BTP-IIC-2Cl

In a dry two-necked 50 mL flask, compound **1a** (410 mg, 0.36 mmol), compound **2** (91 mg, 0.40 mmol) and compound **3** (105 mg, 0.40 mmol) were dissolved in anhydrous chloroform (20 mL). A solution containing pyridine (1 mL) in anhydrous chloroform (4 mL) was added dropwise to the mixture at 0 °C under an argon atmosphere. After stirring at 0 °C for 1 h, the mixture was stirred at 65 °C for another 24 h. After that, the mixture was poured into methanol and filtered. The residue was purified with column chromatography on silica gel using dichloromethane/petroleum ether (2/1, *v*/*v*) as the eluent to give a dark blue solid **BTP-IIC-2Cl** (140 mg, 24% yield). ^{1}H NMR (600 MHz, $CDCl_3$) δ 9.19 (s, 1H), 9.14 (s, 1H), 9.06 (s, 1H), 8.74 (s, 1H), 8.28 (s, 1H), 7.96 (s, 1H), 4.90 - 4.72(m, 4H), 3.29 - 3.15 (m, 8H), 2.21 - 2.10 (m, 2H), 1.93 - 1.80 (m, 4H), 1.56 - 1.45 (m, 4H), 1.42 - 1.33 (m, 4H), 1.33 - 1.19 (m, 26H), 1.19 - 0.76 (m, 36H), 0.76 - 0.60 (m, 12H). ^{13}C NMR (150 MHz, $CDCl_3$) δ 186.39, 186.29, 166.48, 166.27, 158.71, 158.66, 154.91, 154.13, 147.65, 147.61, 145.64, 145.47, 144.95, 141.67, 139.67, 139.32, 138.85, 137.95, 137.75, 137.30, 137.25, 136.48, 136.42, 136.15, 136.05, 135.77, 134.87, 134.31, 134.06, 133.80, 132.03, 132.01, 131.20, 131.19, 126.98, 125.11, 120.10, 119.68, 119.63, 117.93, 115.28, 115.17, 114.70, 114.63, 113.98, 113.71, 70.01, 68.96, 55.97, 39.41, 32.05, 31.79, 31.76, 31.74, 31.43, 31.33, 30.67, 30.54, 30.01, 30.00, 29.96, 29.79, 29.75, 29.65, 29.58, 29.47, 29.47, 28.23, 28.10, 28.03, 27.97, 25.71, 25.64, 25.47, 25.35, 24.72, 23.00, 22.95, 22.93, 22.82, 22.66, 22.62, 14.33, 14.26, 14.22, 14.19, 14.17, 13.98, 13.95, 13.91. MS (MALDI-TOF) *m/z* calcd. for $C_{93}H_{106}Cl_2N_9O_4S_5$ $[M + H]^+$: 1642.6348, found: 1642.6683.

Synthesis of BTP-IIC-BO-2Cl

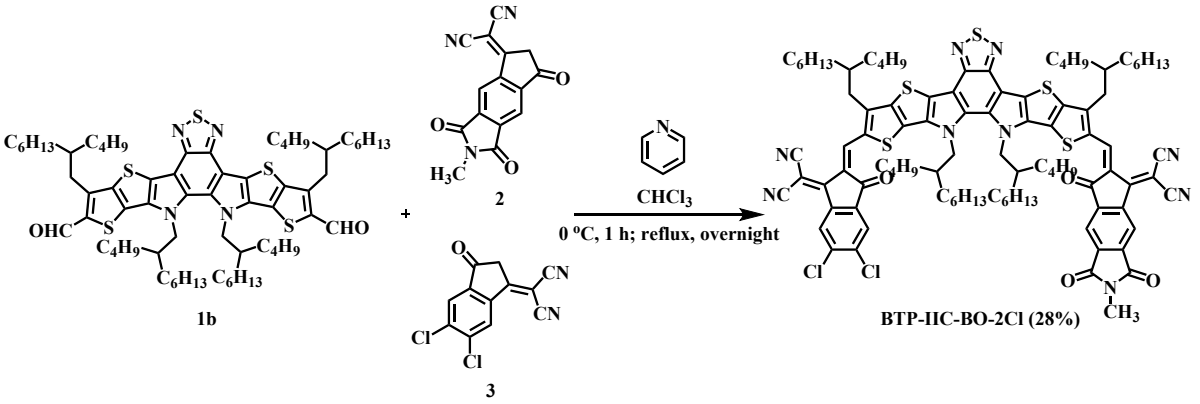

In a dry two-necked 50 mL flask, compound **1b** (404 mg, 0.35 mmol), compound **2** (86 mg, 0.38 mmol) and compound **3** (100 mg, 0.38 mmol) were dissolved in anhydrous chloroform (20 mL). A solution containing pyridine (1 mL) in anhydrous chloroform (4 mL) was added dropwise to the mixture at 0 °C under an argon atmosphere. After stirring at 0 °C for 1 h, the mixture was stirred at 65 °C for another 24 h. After that, the mixture was poured into methanol and filtered. The residue was purified with column chromatography on silica gel using dichloromethane/petroleum ether (2/1, *v*/*v*) as the eluent to give a dark blue solid **BTP-IIC-BO-2Cl** (162 mg, 28% yield). ^{1}H NMR (600 MHz, $CDCl_3$) δ 9.22 (s, 1H), 9.16 (s, 1H), 9.10 (s, 1H), 8.79 (s, 1H), 8.10 (s, 1H), 7.96 (s, 1H), 4.87 - 4.70 (m, 4H), 3.27 (s, 3H), 3.18 (t, *J* = 7.5 Hz, 4H), 2.19 - 2.01 (m, 4H), 1.53 - 0.73 (m, 76H), 0.73 - 0.56 (m, 12H). ^{13}C NMR (150 MHz, $CDCl_3$) δ186.27, 186.17, 166.46, 166.25, 158.90, 154.58, 153.76, 147.71, 147.67, 145.80, 145.58, 144.92, 141.67, 139.64, 139.27, 138.82, 137.83, 137.64, 137.26, 137.05, 136.44, 136.23, 136.14, 134.88, 134.63, 134.33, 132.07, 131.25, 126.94, 125.07, 120.20, 119.77, 119.59, 117.87, 115.49, 115.38, 114.74, 114.68, 113.91, 113.66, 70.04, 69.00, 56.06, 56.01, 40.35, 40.17, 39.42, 34.85, 34.77, 33.70, 33.67, 33.42, 33.39, 32.27, 31.97, 31.76, 31.74, 31.72, 30.75, 30.71, 30.68, 30.57, 30.51, 29.77, 29.61, 29.56, 28.93, 28.09, 28.04, 27.98, 26.69, 25.81, 25.75, 25.69, 24.71, 23.12, 22.94, 22.91, 22.78, 22.62, 14.23, 14.19, 14.19, 13.93, 13.91, 13.89.MS (MALDI-TOF) *m/z* calcd. for $C_{95}H_{110}Cl_2N_9O_4S_5$ $[M+H]^+$: 1670.6661, found: 1670.6073.

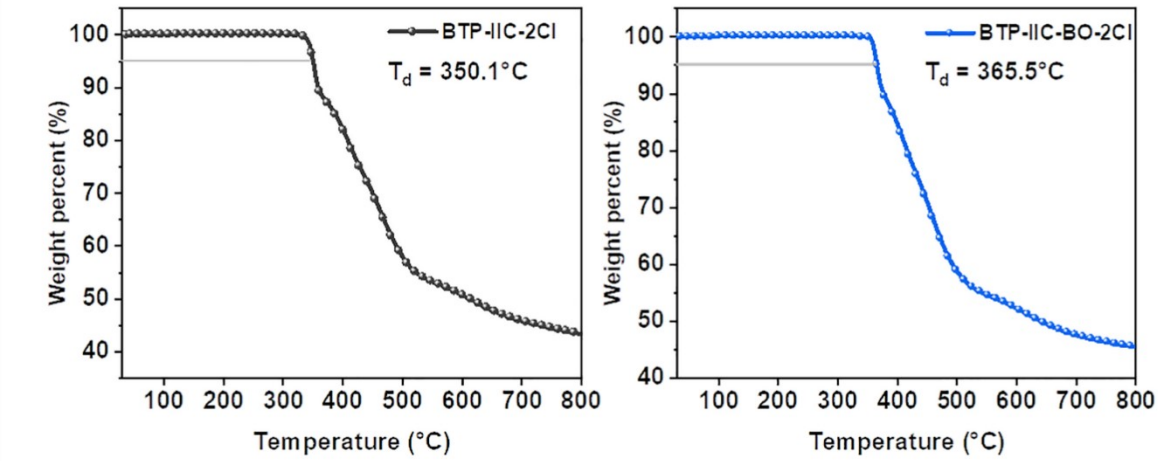

Figure S1. The TGA curves of BTP-IIC-2Cl and BTP-IIC-BO-2Cl.

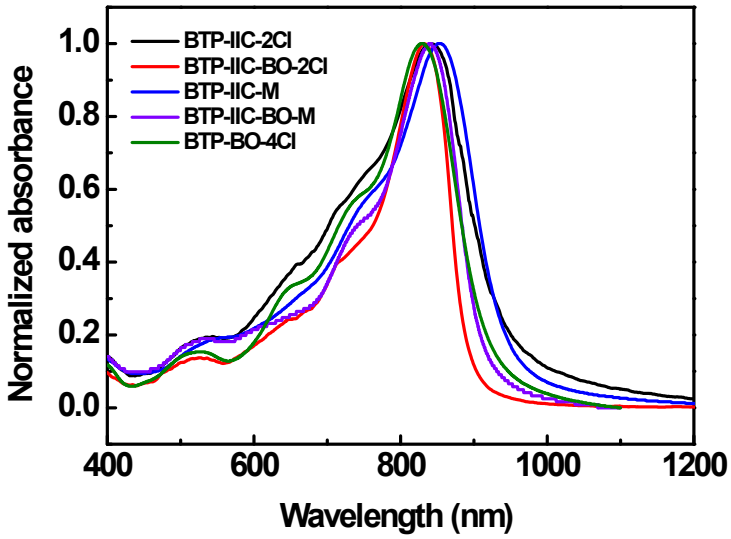

Figure S2. UV-vis-NIR absorption spectra of BTP-IIC-2Cl, BTP-IIC-BO-2Cl, BTP-IIC-M, BTP-IIC-BO-M and BTP-BO-4Cl in thin films

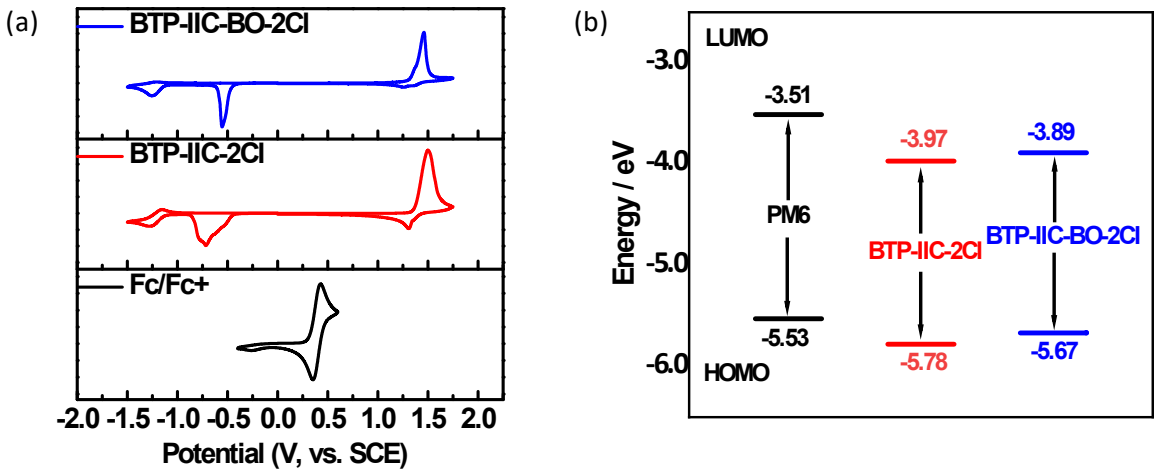

Figure S3. (a) Cyclic voltammetry curves and (b) energy levels determined by CV measurement of BTP-IIC-2Cl and BTP-IIC-BO-2Cl thin films at Pt electrode in 0.1 M Bu_4NPF_6 acetonitrile solution.

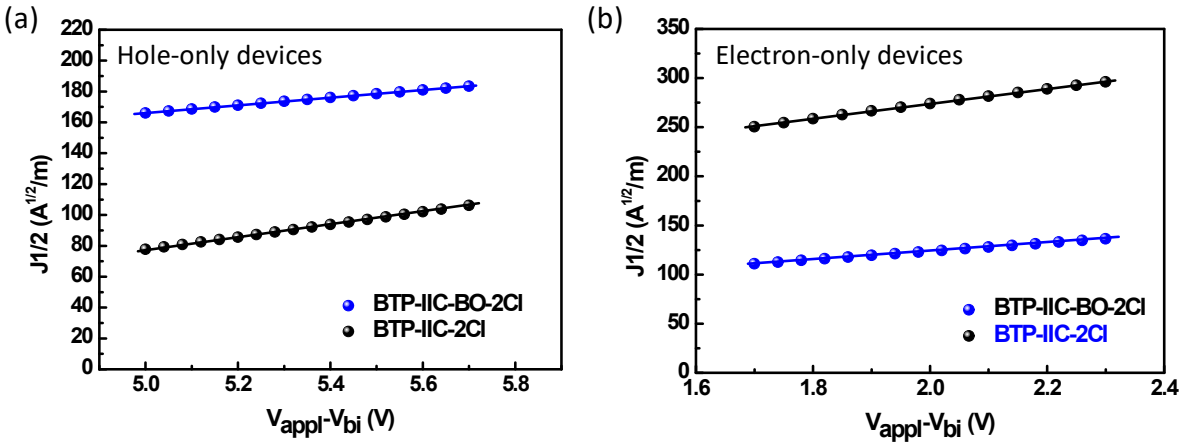

Figure S4. (a) Hole-only devices and (b) electron-only devices, fabricated by PM6:BTP-IIC-2Cl and PM6:BTP-IIC-BO-2Cl thin films.

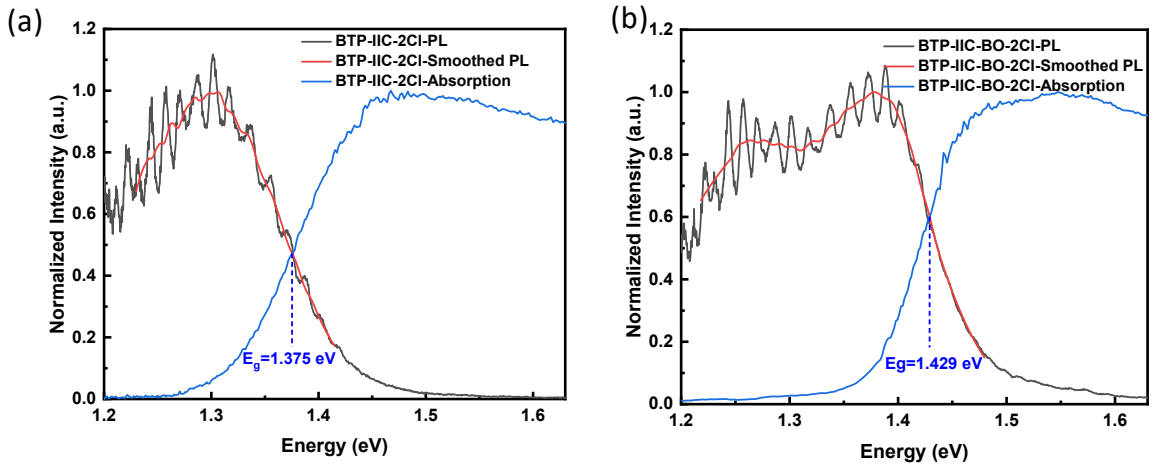

Figure S5. Absorption and photoluminescence curves of (a) PM6:BTP-IIC-2Cl and (b) PM6:BTP-IIC-BO-2Cl blends

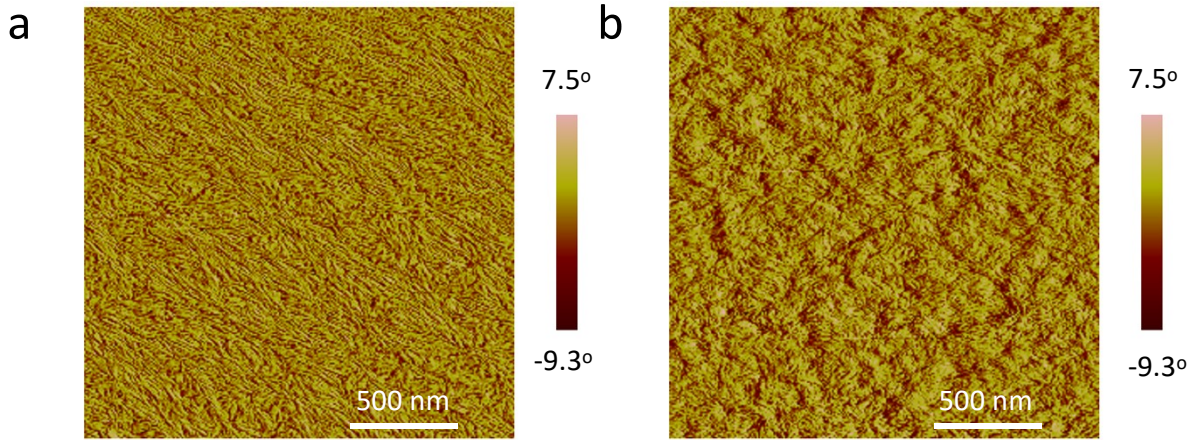

Figure S6. AFM phase images of (a) PM6:BTP-IIC-2Cl and (c) PM6:BTP-IIC-BO-2Cl blends.

Table S1. Photovoltaic parameters of the OSCs based on PM6:**BTP-IIC-2Cl** with different weight ratio.

PM6:BTP-IIC-2Cl [w/w]	V_{oc} (V)	J_{sc} (mA/cm^2)	FF (%)	PCE (%)
1:1.0	0.86	23.89	66.15	13.65
1:1.2	0.86	24.71	64.74	13.68
1:1.4	0.86	24.04	61.35	12.62

Table S2. Photovoltaic parameters of the OSCs based on PM6:**BTP-IIC-2Cl=1:1.2** with different additive content and different annealing temperature.

Additive DIO (Vol%)	Annealing temp. (°C)	V_{oc} (V)	J_{sc} (mA/cm^2)	FF (%)	PCE (%)
0.25	60	0.843	25.42	70.28	15.06
	90	0.835	25.78	70.69	15.23
	120	0.821	26.03	69.73	14.89
0.50	60	0.827	26.18	70.16	15.18
	90	0.824	25.79	69.01	14.66
	120	0.823	26.41	69.90	15.19
0.75	60	0.830	25.77	73.93	15.82
	90	0.820	26.92	76.38	16.86
	120	0.810	25.74	70.10	14.62
1.00	60	0.829	24.41	73.99	14.97
	90	0.833	24.69	74.51	15.32
	120	0.825	24.99	72.03	14.85

Table S3. Photovoltaic parameters of the OSCs based on PM6:**BTP-IIC-BO-2Cl** with different weight ratio.

PM6:BTP-IIC-BO-2Cl [w/w]	V_{oc} (V)	J_{sc} (mA/cm^2)	FF (%)	PCE (%)
1:1	0.89	20.54	73.34	13.52
1:1.2	0.90	21.87	71.02	13.86
1:1.4	0.89	20.56	72.46	13.31

Table S4. Photovoltaic parameters of the OSCs based on PM6:**BTP-IIC-BO-2Cl=1:1.2** with different additive content and different annealing temperature.

Additive CN (Vol %)	Annealing temp. (°C)	V_{oc} (V)	J_{sc} (mA/cm^2)	FF (%)	PCE (%)
0.3	60	0.88	20.77	77.33	14.12
	90	0.88	21.86	77.58	14.94
	120	0.87	22.52	75.14	14.71
	150	0.85	22.71	75.39	14.51
0.6	60	0.88	21.51	75.58	14.27
	90	0.88	21.96	78.83	15.16
	120	0.87	22.46	79.03	15.36
	150	0.85	22.97	75.72	14.69
0.9	60	0.87	18.98	76.17	12.62
	90	0.88	21.23	78.03	14.56
	120	0.87	21.55	79.06	14.83
	150	0.85	21.59	77.05	14.17

Table S5. Photovoltaic parameters of exciton dissociation, charge-carriers collection, and recombination for the NFAs-based OSCs, and hole and electron mobilities of PM6:BTP-IIC-2Cl and PM6:BTP-IIC-BO-2Cl thin films.

Acceptor	J_{sat} (mA/cm^2)[a]	J_{ph}^{s} (mA/cm^2)[b]	J_{ph}^{m} (mA/cm^2)[c]	P_{diss} (%)[d]	P_{coll} (%)[e]
BTP-IIC-2Cl	27.49	26.56	21.66	96.62	78.79
BTP-IIC-BO-2Cl	24.86	23.66	17.94	95.17	72.16

[a] saturation photocurrent density; [b] Photocurrent density under short circuit condition; [c] Photocurrent density under maximum power output condition; [d] exciton dissociation probability calculated by J_{ph}^{s}/J_{sat}; [e] Carrier collection probability calculated by J_{ph}^{m}/J_{sat}.

Table S6. Summary of peak location, π-π stacking distances, and crystal coherence length for neat films of NFAs and their blend films in the IP direction.

Materials	Lamellar stacking in IP	
	Peak location [Å^{-1}]	Lamellar stacking distance [Å]
BTP-IIC-2Cl	0.39	16.03
BTP-IIC-BO-2Cl	0.43	14.65
PM6:BTP-IIC-2Cl	0.30	21.04
PM6:BTP-IIC-BO-2Cl	0.30	20.76
PM6	0.27	22.95

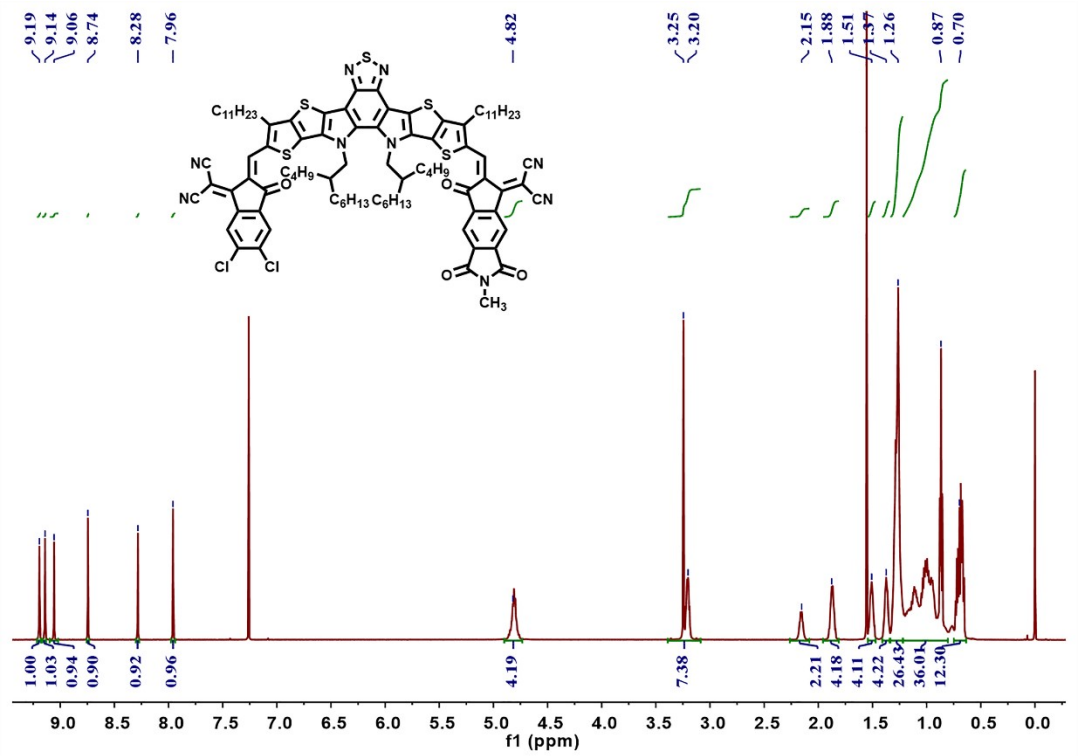

Figure S7. ^{1}H NMR spectrum of **BTP-IIC-2Cl** in $CDCl_3$

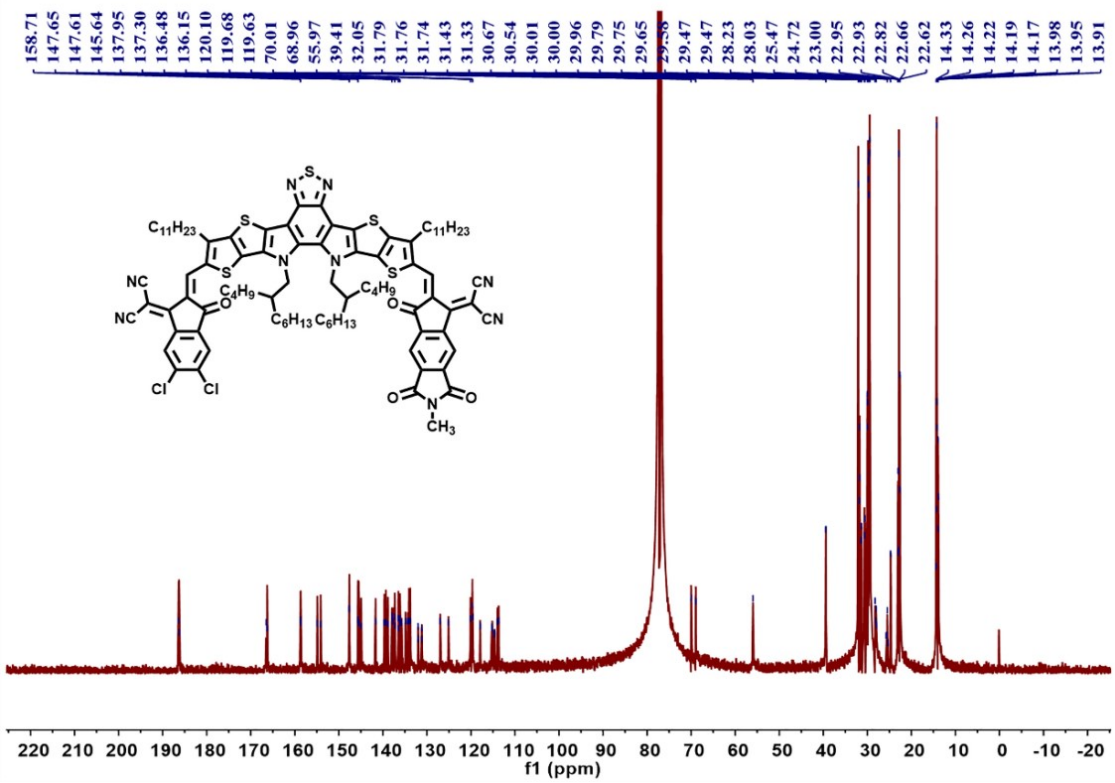

Figure S8. ^{13}C NMR spectrum of **BTP-IIC-2Cl** in $CDCl_3$

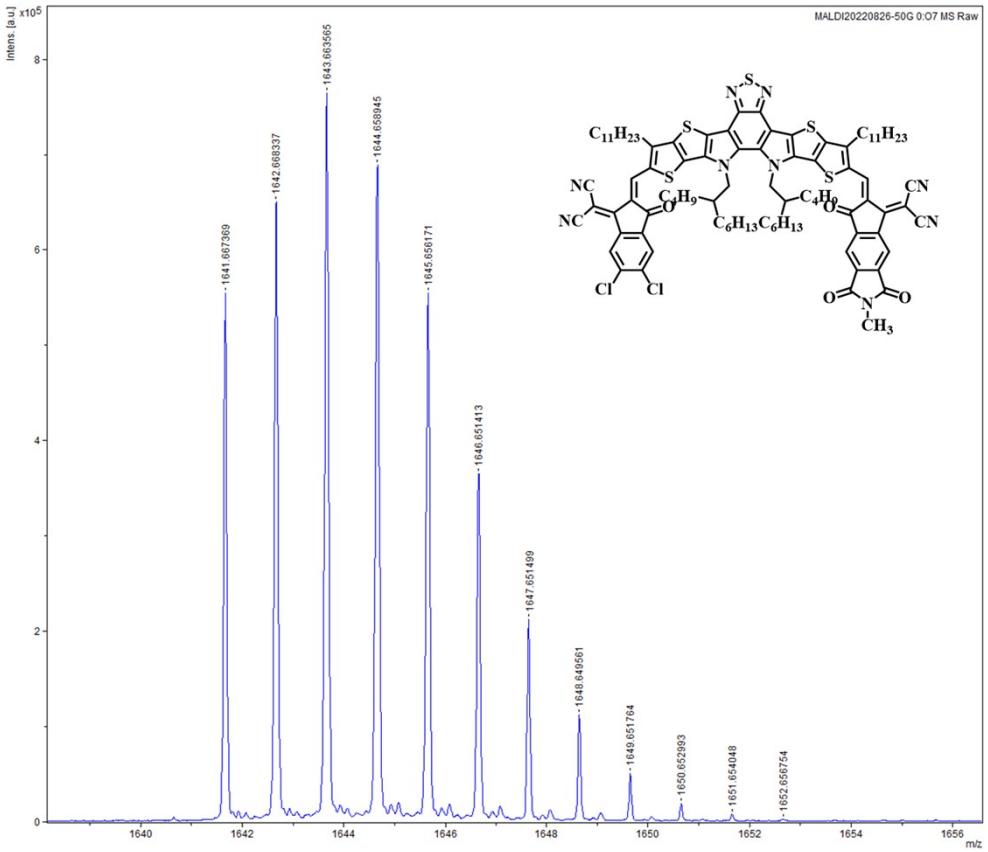

Figure S9. MALDI-TOF MS analyses of **BTP-IIC-2Cl**

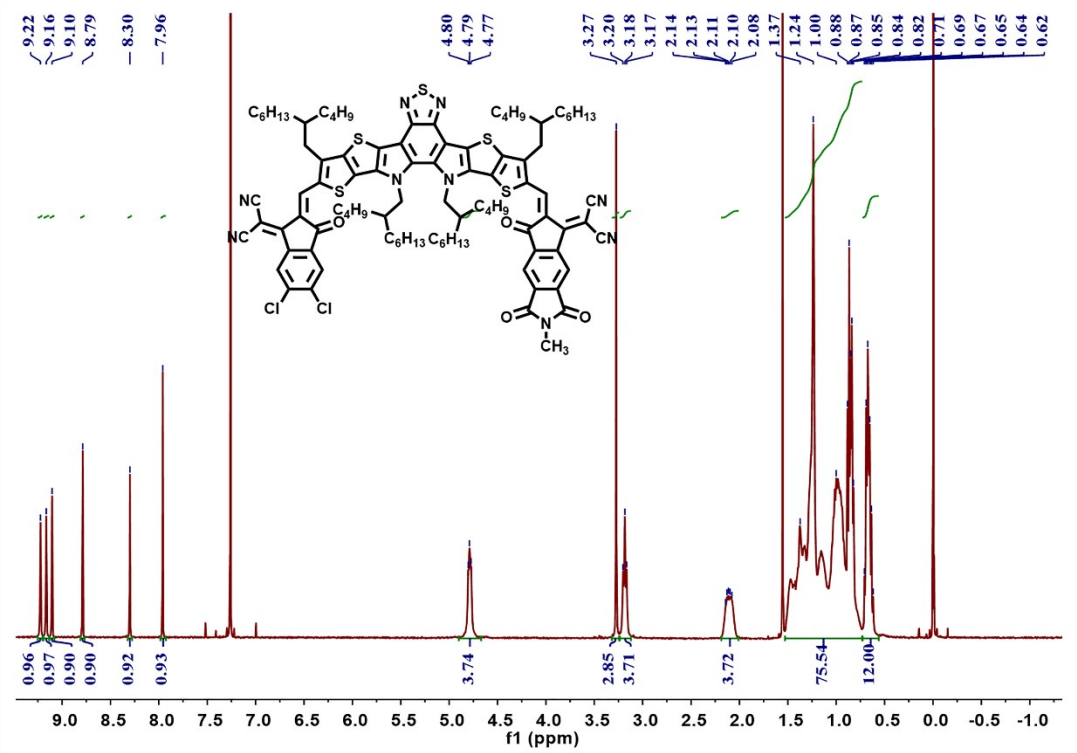

Figure S10. ^{1}H NMR spectrum of **BTP-IIC-BO-2Cl** in $CDCl_3$

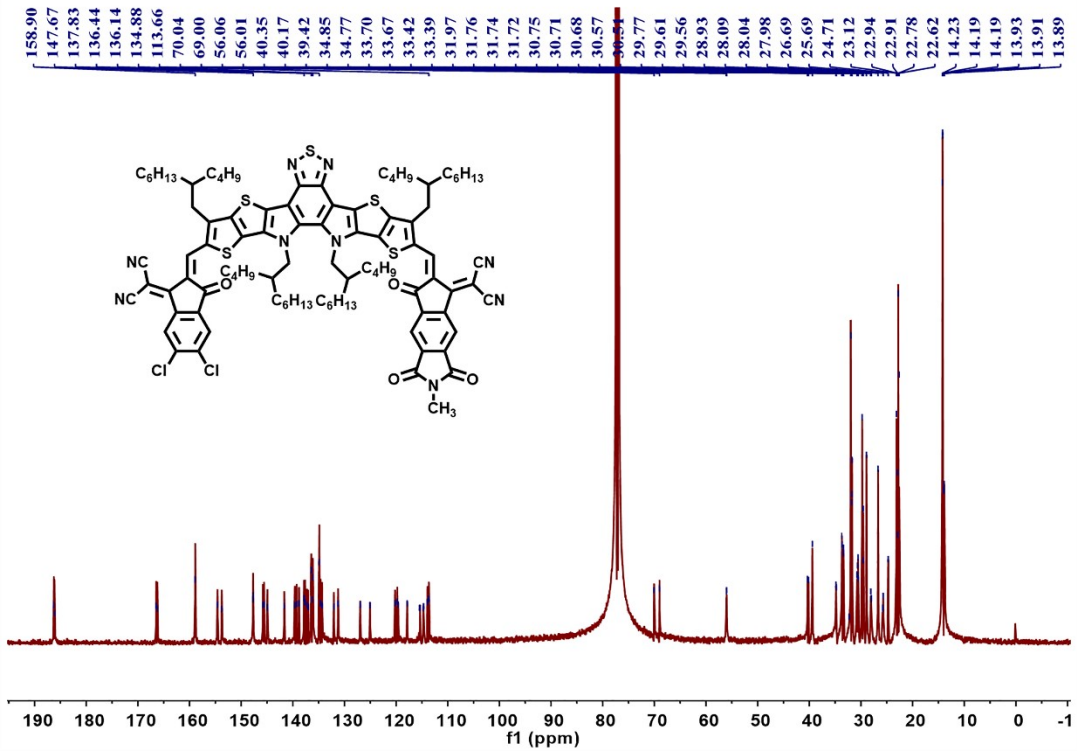

Figure S11. ^{13}C NMR spectrum of **BTP-IIC-BO-2Cl** in $CDCl_3$

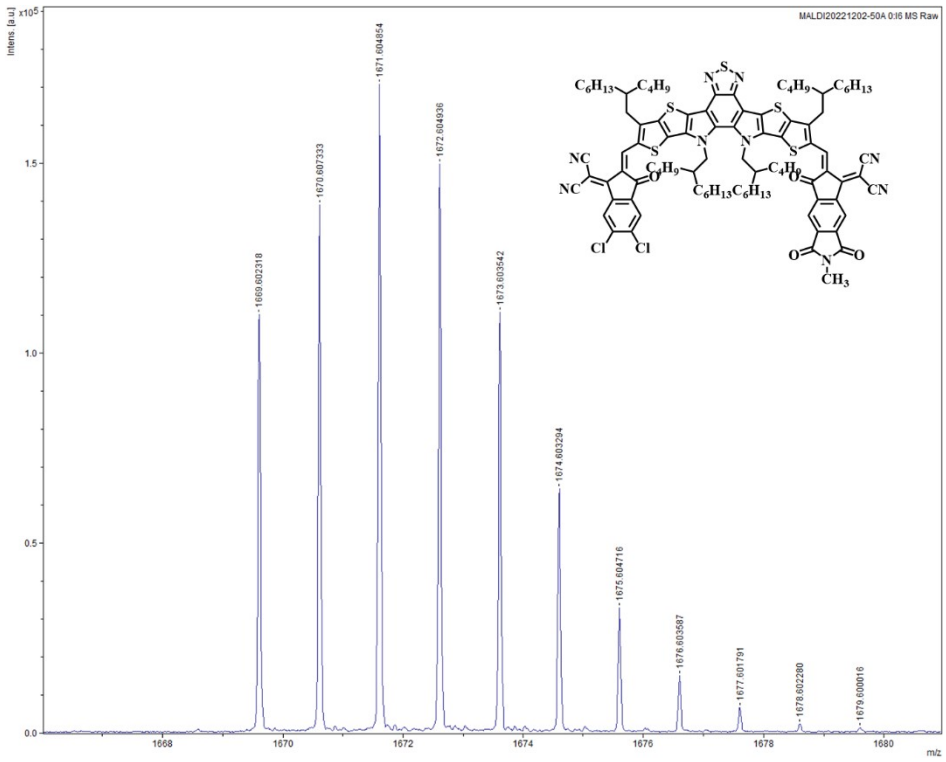

Figure S12. MALDI-TOF MS analyses of **BTP-IIC-BO-2Cl**

References

1. Y. Li, H. Meng, J. Huang and C. Zhan, *ACS Appl. Mater. Interfaces*, 2020, **12**, 50541-50549.
2. S. Feng, C. Zhang, Y. Liu, Z. Bi, Z. Zhang, X. Xu, W. Ma and Z. Bo, *Adv. Mater.*, 2017, **29**, 1703527.
3. C. Li, X. Zhang, N. Yu, X. Gu, L. Qin, Y. Wei, X. Liu, J. Zhang, Z. Wei, Z. Tang, Q. Shi and H. Huang, *Adv. Funct. Mater.*, 2022, **32**, 2108861.
4. K. Vandewal, J. Benduhn and V. C. Nikolis, *Sustain. Energy Fuels*, 2018, **2**, 538-544.
5. U. Rau, B. Blank, T. C. M. Müller and T. Kirchartz, *Appl. Phys. Rev.*, 2017, **7**, 044016.
6. M. E. Ziffer, S. B. Jo, H. Zhong, L. Ye, H. Liu, F. Lin, J. Zhang, X. Li, H. W. Ade, A. K. Y. Jen and D. S. Ginger, *J. Am. Chem. Soc.*, 2018, **140**, 9996-10008.
7. T. Saito, S.-i. Natsuda, K. Imakita, Y. Tamai and H. Ohkita, *Sol. RRL*, 2020, **4**, 2000255.
8. J. Yuan, Y. Zhang, L. Zhou, G. Zhang, H.-L. Yip, T.-K. Lau, X. Lu, C. Zhu, H. Peng, P. A. Johnson, M. Leclerc, Y. Cao, J. Ulanski, Y. Li and Y. Zou, *Joule*, 2019, **3**, 1140-1151.
9. S. Shi, S. Zhang, Z. Xue, X. Yao, G. Zhang, J. Gao, Y. Li, X. Tu, S. Zhang, C. Zhang, Z. Liu, Z. Tang, H. Zhong, W. Li and Z. Fei, *ACS Appl. Mater. Interfaces*, 2023, **15**, 12119-12126.
10. M. Zhang, X. Guo, W. Ma, H. Ade and J. Hou, *Adv. Mater.*, 2015, **27**, 4655-4660.